Multiscale simulation of the intralaminar failure of graphene nanoplatelets reinforced fibers laminate composite materials

Matteo Basso[1], Wiyao Azoti[2,3*], Hana Elmarakbi[4,5]and Ahmed Elmarakbi[5]

[1]Centro Ricerche Fiat S.C.p.A, Group Materials Labs, Polymers & Glass, Composites, Pomigliano d'Arco, Italy.
[2]ECAM Strasbourg-Europe, School of Engineering, Schiltigheim, 67300, France.
[3]ICube Laboratory, CNRS UMR 7357, University of Strasbourg, Strasbourg, 67000 France.
[4]St Anthony's Academy, Sunderland SR2 7JN, UK
[5]Automotive Composites, Department of Mechanical and Construction Engineering, Faculty of Engineering and Environment, Northumbria University, Newcastle NE1 8ST, UK.
[*]Correspondence to: Wiyao Azoti (wiyao.azoti@ecam-strasbourg.eu)

ABSTRACT

This paper presents a multiscale approach to derive the intralaminar properties of graphene nanoplatelets (GNPs)-based polymeric composites reinforced by short glass fibers (SGFs) and unidirectional carbon fibers (UCFs). The approach accounts for the debonding at the interface of a 2-phases GNPs/polymer matrix using a cohesive model. The resulting composite is used within a 3-phases nanocomposite consisting either of a GNPs/polyamide/SGFs or a GNPs/epoxy/UCFs nanocomposite. Experiments are performed for determining the interlaminar fracture toughness in Mode I for the GNPs/epoxy/UCFs. Results show that the aspect ratio AR of GNPs influences the effective Young modulus which increases until a threshold. Also, the addition of the GNPs increases up to 10% the transverse Young modulus and up to 11% the shear modulus as well as up to 16% the transverse tensile strength useful in crashworthiness performance. However, the nanocomposite behavior remains fiber-dominant in the longitudinal direction. This leads to a weak variation of the mechanical properties in that direction. Due to the well-known uniform dispersion issues of GNPs, the intralaminar fracture toughness G_{IC} has decreased up to 8.5 % for simulation and up to 2.4% for experiments while no significant variation of the intralaminar stress distribution is obtained compared to a nanocomposite without GNPs.

INTRODUCTION

Environmental sustainability represents one of the major driving forces for innovation from the automotive sector, according to the European Commission's regulation for CO_2 emissions. Due to the high emphasis on greenhouse gas reductions and improving fuel efficiency, stringent values for fuel economy are set depending on the average vehicle's weight. For horizon 2020, EU has fixed the target in 95g CO_2/km and for horizon 2025, this target is set to 75g CO_2/km [1]. Omitting powertrain changes, the use of lighter structural and semi-structural materials (including polymer-based materials such as glass fibers and carbon fibers reinforced plastic (GFRP, CFRP) is emerging as the most promising way to reduce CO_2 emissions of vehicles (that are proportional to fuel consumption). The specific material selection is dependent upon performance requirements as well as the location of the automotive parts and their

functional role in the car. Alongside the demand for reductions in exhaust emissions, government regulations also mandate increased safety requirements. Thus, advanced materials must guarantee the fundamental performance of vehicles, with a key feature in functionality being crashworthiness. This guarantee often depends on technical design specifications and the engineering of innovative solutions. One strategy that can be applied is that of multifunctional design with the combination of light structures and nanostructured materials manufactured with additive nanofillers, such as carbon nanotubes or graphene nanoplatelets (GNPs). The approach of multifunctional design applied to automotive components has not been widely documented (at the authors' best knowledge). GNPs have shown exceptional physical and thermomechanical properties, a high surface/volume ratio [2-4], as well as lower filler content, which make GNPs a promising candidate for developing the next-generation of polymer composites. In addition, graphene related materials increase the stiffness, toughness, thermal conductivity, electrical performances and mechanical behavior of polymer resins by a large margin [5-14].
The durability of such multi-phasic composites depends on the properties of their constituents and their microstructural arrangement as well as their ability to withstand mechanical fracture across the length scale. Earlier works in the estimation of effective fracture toughness for multi-phasic composites are provided by Rao [15]. From a numerical aspect, multiscale models have been developed to enhance the accuracy of the fracture mechanism in a multiphasic composites [16] as well as to predict the crack's propagation across the volume boundaries in arbitrary directions[17]. A mode-I fracture test is conducted experimentally by Saghafi et al. [18] to investigate the effect of nanofibers on the fracture behavior of carbon/epoxy laminates. Significant research literature has been developed in relation to studying the stiffness, strength and fracture toughness of nanocomposites versus the inclusion's size, interfacial behavior and inclusion loading (i.e volume fraction [19]). With regards to stiffness, Ji et al. [20] have shown that below a certain threshold of nanoparticle size (for instance 30 nm) there is a significant dependence on the predicted Young modulus versus the volume fraction. Indeed, for a considered volume fraction of nanoparticles, the elastic modulus increases with a decrease of the particle size. The same observation has been obtained in terms of the strength for Silica/Polyamide PA6 nanocomposites for which the addition of particles has led to an increase of the strength while smaller particles have given better reinforcement [21]. Depending on the toughening mechanisms, the particle size has an important effect on the composite toughness, which can be increased or reduced with increasing particle size [19]. The volume fraction of nanoparticles has double trends on the fracture resistance as well as the impact toughness: Indeed, the higher the volume fraction, the better the performance of the composite compared to the neat matrix [22]. The interfacial adhesion between particles and matrix also play a significant role on the fracture toughness as reported by Ou et al [23]. Cohesive interfacial models have been proposed by Fedele and Milani [24] to study the delamination of fibers reinforced composites for masonries. The derivation of the homogenized properties is proposed by Sejnoha and Zeman [25] for random distribution of fibers. The homogenized properties of such composites and the delamination phenomena have been investigated through analytical multi-step approaches and numerical finite element FE methods by Cecchi et al. [26, 27]. For a Silica/Polyamide PA6 6 nanocomposite, untreated particles lead to a decrease monotonically of the impact toughness with increasing particle volume fraction probably due to the poor interfacial adhesion between silica and Polyamide PA6 6 [23]. Recently, a multiscale derivation of the nonlinear behavior of GNPs based nanocomposites showing imperfect interfacial has been proposed by Azoti et al. [28, 29].

However, open challenges [30, 31] still remain in terms of the capability of GNPs to interlock with the polymer chain in order to generate an extensive and strong interface zone. In addition, the problem of the particles' clustering is important, especially during the industrial processes for mass production with the difficulty of applying advanced techniques of dispersion as in a lab environment.

This work aims to study the capability of GNPs to enhance the mechanical properties of short glass fibers (SGFs) thermoplastic composites and unidirectional carbon fibers (UCFs) thermoset composites. Both composites are used in automotive components such as the bumper beam, whose outer faces are manufactured in UCFs reinforced polymer laminates while SGFs reinforced polymer composites are utilised for the inner faces. The automotive sector is currently investigating the contribution of the graphene to enhance composites' crashworthiness absorption [32]. For such a purpose, a micromechanics strategy is used to obtain the behavior of a polymeric matrix functionalized with GNPs and reinforced by SGFs and UCFs. With the purpose of developing a lighter methodology, the clustering of the GNPs are not directly simulated, but rather are represented by the value assumed for a shear strength and a normal strength of the interface based on a cohesive zone model. In other words, the strength values assumed for the interface GNPs/polymer include the clustering of the GNPs in the interlaminar layers. Numerical as well as experimental characterization are performed to study the intralaminar stress distribution for a simulacrum of a bumper beam of automotive. This research work is a fundamental investigation for the R&D unit of FIAT Chrysler Automobile (FCA) with the intention to launch new graphene based lightweighting components in automotive structures. Results indicate that the GNPs increase the effective mechanical response in terms of transversal Young modulus, shear modulus and transverse tensile strength useful in crashworthiness performance. This variation however remains very weak for longitudinal mechanical properties due to low resistance of the interface and the clustering phenomena as well as the difficulty of a uniform dispersion of the GNPs in the polymeric matrix.

THEORETICAL FRAMEWORK OF A MULTISCALE MODELLING OF COMPOSITE MATERIALS

Background on interfacial debonding by cohesive zone model

Cohesive models are used for modelling the debonding process at the interface inclusion-matrix in composite. The material modelling is subdivided into three steps such as [33]:

Linear elastic traction – separation law

The traction stress vector $\mathbf{t}$ is related to the separation (i.e displacement between upper and lower faces of the cohesive element) vector $\boldsymbol{\delta}$ across the cohesive Interface such as:

$$\mathbf{t} = \begin{Bmatrix} t_n \\ t_s \\ t_t \end{Bmatrix} = \begin{bmatrix} K_{nn} & K_{ns} & K_{nt} \\ K_{ns} & K_{ss} & K_{st} \\ K_{nt} & K_{st} & K_{tt} \end{bmatrix} \begin{Bmatrix} \delta_n \\ \delta_s \\ \delta_t \end{Bmatrix} = \mathbf{K}\boldsymbol{\delta} \qquad (1)$$

In Eq.(1), δ_n , δ_s , δ_t represent the components of $\boldsymbol{\delta}$ in the normal, first and second shear directions respectively. t_n , t_s , t_t denote the components of $\mathbf{t}$ in the normal, first and second shear directions respectively. $\mathbf{K}$ is the nominal stiffness matrix. In the case of uncoupled analysis between the normal and

shear components Eq.(1) reads more simply:

$$\mathbf{t} = \begin{Bmatrix} t_n \\ t_s \\ t_t \end{Bmatrix} = \begin{bmatrix} K_{nn} & 0 & 0 \\ 0 & K_{ss} & 0 \\ 0 & 0 & K_{tt} \end{bmatrix} \begin{Bmatrix} \delta_n \\ \delta_s \\ \delta_t \end{Bmatrix} \tag{2}$$

with $K_{ss} = K_{tt}$.

Damage initiation criterion

Maximum stress criterion assumes that the damage occurs when the maximum nominal stress reaches a value of one:

$$\max\left\{\frac{< t_n >}{t_n^0}, \frac{t_s}{t_s^0}, \frac{t_t}{t_t^0}\right\} = 1 \tag{3}$$

with t_n^0 , t_s^0 , t_t^0 the maximum nominal traction in normal only mode and shear only mode, respectively. $< t_n >$ stands for the positive part of the variable t_n **.**

Damage evolution law

It controls the stiffness degradation through the damage parameter D such as $0 \le D < 1$. The damaged stress $\mathbf{t}$ of the traction-separation is related to the undamaged configuration $\bar{\mathbf{t}}$ by:

$$\begin{aligned} t_n &= \begin{cases} (1-D)\,\bar{t}_n, & \bar{t}_n \ge 0 \\ \bar{t}_n & \text{otherwise} \end{cases} \\ t_s &= (1-D)\,\bar{t}_s \\ t_t &= (1-D)\,\bar{t}_t \end{aligned} \tag{4}$$

The evolution of D is given such as:

$$D = \frac{\delta_m^f \left(\delta_m^{\max} - \delta_m^0\right)}{\delta_m^{\max}\left(\delta_m^f - \delta_m^0\right)} \tag{5}$$

where δ_m^f is the effective separation at failure, δ_m^0 is the separation at initiation of damage and $\delta_m^{\max}$ is the maximum separation attained in the complete loading history. It can be based on displacement with linear softening by defining the separation between damage initiation and failure parameter $\left(\delta_m^f - \delta_m^0\right)$.

Effective properties of multi-phasic composite materials

Using the concept of a representative volume element RVE, the micromechanics describes the relationship between a macroscopic homogeneous material and its microscopic heterogeneous phases. The associated boundary-value problems on this RVE are formulated, in the terms of uniform macro field traction vector or linear displacement fields with body. In these conditions, the macroscopic effective stress field and strain field are given by average techniques such as [34]:

$$\begin{cases} \bar{\boldsymbol{\sigma}} = \dfrac{1}{V}\displaystyle\int_V \boldsymbol{\sigma}\, dV \\ \bar{\boldsymbol{\varepsilon}} = \dfrac{1}{V}\displaystyle\int_V \boldsymbol{\varepsilon}\, dV \end{cases} \tag{6}$$

where $\bar{\boldsymbol{\sigma}}$ and $\bar{\boldsymbol{\varepsilon}}$ represent the effective stress and strain of the homogeneous material respectively. $\boldsymbol{\sigma}$ and $\boldsymbol{\varepsilon}$ are the local stress and strain within the RVE respectively. V denotes the volume of the RVE.

For a composite material consisting on a matrix and inclusions phases, Eq. (6) reads:

$$\begin{cases} \bar{\boldsymbol{\sigma}} = \bar{\boldsymbol{\sigma}}_m + \bar{\boldsymbol{\sigma}}_I \\ \bar{\boldsymbol{\varepsilon}} = \bar{\boldsymbol{\varepsilon}}_m + \bar{\boldsymbol{\varepsilon}}_I \end{cases} \tag{7}$$

where $\bar{\bullet}_m$ and $\bar{\bullet}_I$ are the effective properties of variable $\bullet$ related to the matrix and the inclusions respectively. From a computational view point, the macroscopic effective stress within the matrix can be obtained by:

$$\bar{\boldsymbol{\sigma}}_m = \frac{\displaystyle\sum_{j=1}^{N} IVOL[j]\, \boldsymbol{\sigma}_m[j]}{\displaystyle\sum_{j=1}^{N} IVOL[j]} \tag{8}$$

with $IVOL$ denoting the integration point volume and N representing the total number of Gauss integration points on the considered matrix set and j is the summation index. $\boldsymbol{\sigma}_m$ is stress output field. In the sequel, the micromechanics analysis will be performed using the software Digimat [33].

Assumptions for the modelling of the GNPs reinforced nanocomposites

The following assumptions are made:

- The GNP are dispersed within the matrix (thermoplastic or thermoset) for sake of enhancement of the strength and the fracture toughness i.e. resistance to delamination. The fracture toughness depends on the matrix located between two adjacent plies of the laminate as shown for the UCFs reinforced polymer laminates by Figure 1. In order to evaluate the enhancement due to the GNPs onto the matrix fracture toughness and strength, it is assumed that the damage is basically determined by debonding between platelets and matrix. The cracks evolve primarily due to the debonding between nanoparticles and matrix [19]. Therefore, the energy for the debonding of nanoparticles is equivalent to matrix fracture toughness. The debonding curve is equal to the curve until break. The maximum value of the load is equivalent to the value of the material's yield stress. Figure 2 gives an illustration

of the debonding process between the inclusions and matrix in a composite.

- For GNP/Polyamide PA6 debonding modelling, a cohesive zone model is described through a traction-separation law. The variables such as the maximum nominal stress at the damage initiation, the stiffness of the interface and the damage evolution law until the complete separation need to be provided as input. The area under the curve (Figure 2) of the damage's evolution represents the separation energy between particles and matrix. Based on data from works by Safaei et al. [35] and Huang et al. [36], values in Table 1 correspond to an interface that has average strength (medium interface), taking into account the difficulty to evenly disperse the nanoparticles. An interface with average strength also considers that the surface of the nanoplatelets is not treated in a perfect way in an industrial process. The traction-separation stiffness's are given such as $K_{nn} = 2500\ \text{MPa}$ and $K_{ss} = K_{tt} = 3200\ \text{MPa}$. The material properties and the volume fraction of GNPs used in this work are given in Table 2.

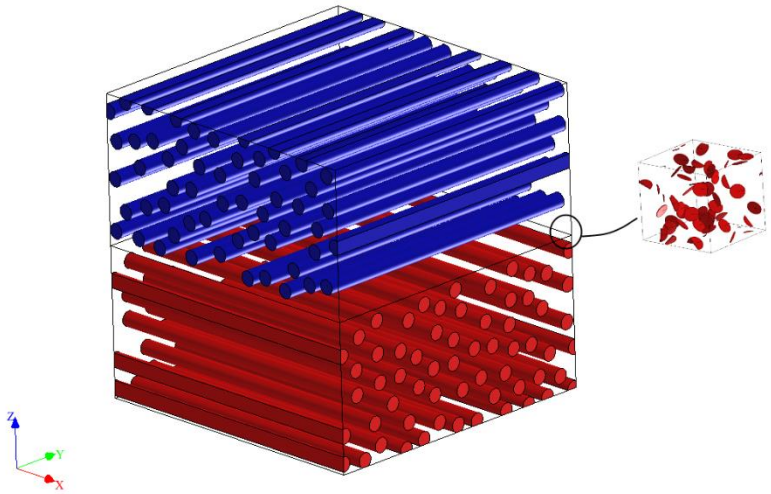

FIGURE 1: Illustration of the GNPs reinforced matrix between the plies of a laminate.

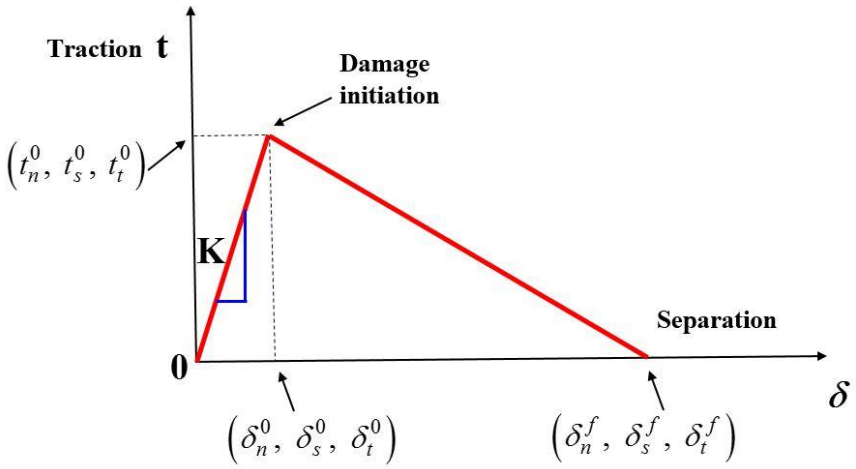

FIGURE 2: Illustration of the debonding process in composite.

TABLE 1: Values of the strength at the GNPs/matrix interface

	Strong interface [MPa]	Medium interface [MPa]	Weak interface [MPa]
Shear Mode $t_s^0 = t_t^0$	110	96	30
Normal Mode t_n^0	170	150	40

TABLE 2: Material properties and volume fraction % vol for components [37-40]

	Thermoplastic with Short Glass Fibers SGFs	
Characteristics	Matrix: Polyamide PA6	SGFs
Density [g/cm3]	1.13	2.49
Poisson's ratio	0.39	0.22
Young modulus [MPa]	2000	89000
Tensile Strength [MPa]	-	4750
Tensile Strain at yield	3.5 %	-
Compressive Strength [MPa]	-	4500 MPa
Yield Stress [MPa]	60.5	-
Hardening Modulus [MPa]	63	-
Hardening Model	Power law	-
Hardening exponent	0.4	-
Aspect Ratio	-	23.5
	Epoxy with Unidirectional Carbon Fibers UCFs	
Characteristics	Matrix: Epoxy	UCFs
Density [g/cm3]	1.2	1.76
Poisson's ratio	0.34	-
Young modulus [MPa]	3407MPa	230 GPa
Tensile Strength [MPa]	85 MPa	3530 MPa
Tensile Strain	-	1.5%
	Nanofillers for functionalized matrix	
		Volume fraction Vf%
Characteristics	GNP	GNPs/PA6 /SGFs	GNPs/Epoxy/UCFs
Density [g/cm3]	2.2	GNPs (1%)/PA6	GNPs (2%)/Epoxy (36%)/UCFs
Poisson's ratio	0.22	(54%)/SGFs (45%)	(62%)
Young modulus [GPa]	1000		
Tensile Strength [GPa]	5		
Thickness [nm]	10		
Average lateral size [μm]	10-60		

RESULTS AND DISCUSSION

Two-phases GNPs reinforced polymer nanocomposites

GNPs/Polyamide PA6 nanocomposites

The Young modulus of GNPs and their volume fraction are the selected design parameters. For a fixed AR such as AR=0.054, different Young modulus (E_{GNP1} = 1000 GPa, E_{GNP2} = 700 GPa and E_{GNP3} = 400 GPa) are studied for a perfectly bounded interface GNP/Polyamide PA6 composite. The value of Young modulus E_{GNP} = 1000 GPa is closed to the in-plane GNPs values found in the works by Lee et al. [41], Cho et al. [42] (2007), Xiao et al. [43]. Different volumes fractions are analyzed. The figure 3 gives an illustration of the microstructure of the simulated composite for a volume fraction of Vf=1%, 2% and 5%. The results of the simulation are given by the Table 3.

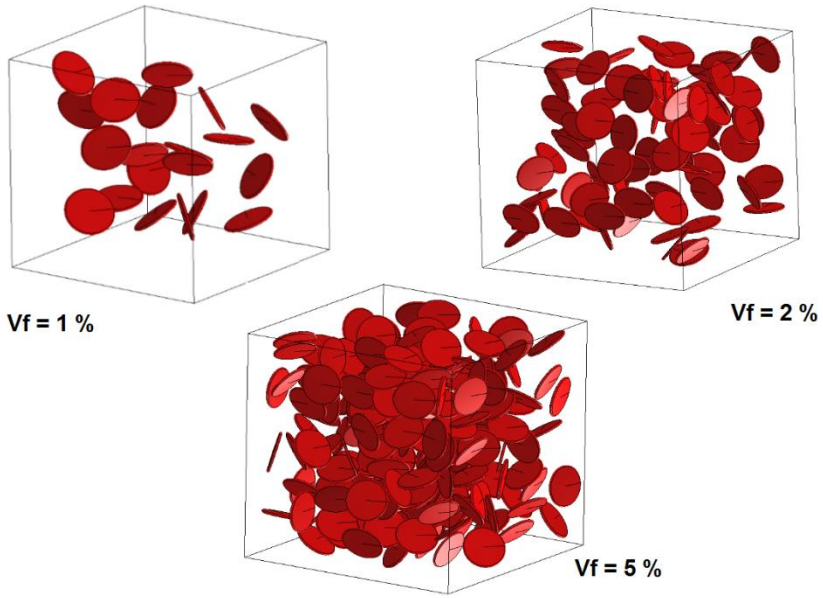

FIGURE 3: Simulation of different volume fractions of GNPs.

TABLE 3: Effective properties of a GNPs/Polyamide PA6 composite versus the GNPs volume fraction

Young modulus E_{GNP} [GPa]	1000	700	400
Vf GNP = 1%			
Effective Young Modulus E [MPa]	2277	2284	2279
Effective Shear Modulus G [MPa]	786	775	773
Effective Poisson's ratio ν	0.38	0.38	0.38
Density ρ	1.14	1.14	1.14
Vf GNP = 2%			
Effective Young Modulus E [MPa]	2476	2435	2446
Effective Shear Modulus G [MPa]	844	846	842
Effective Poisson's ratio ν	0.38	0.38	0.38
Density ρ	1.14	1.14	1.14

Vf GNP = 5%			
Effective Young Modulus E [MPa]	3169	3135	3072
Effective Shear Modulus G [MPa]	1044	1034	1014
Effective Poisson's ratio ν	0.38	0.38	0.38
Density ρ	1.14	1.14	1.14

The effective stress-strain behavior, with respect to the variation of the volume fraction, is presented in Figure 4. The effective Young modulus E increases when the volume fraction vf becomes higher. It must be highlighted that the introduction in the matrix of the 1% of the GNPs gives an enhancement of about 13 % of the stiffness of the matrix polyamide PA6.

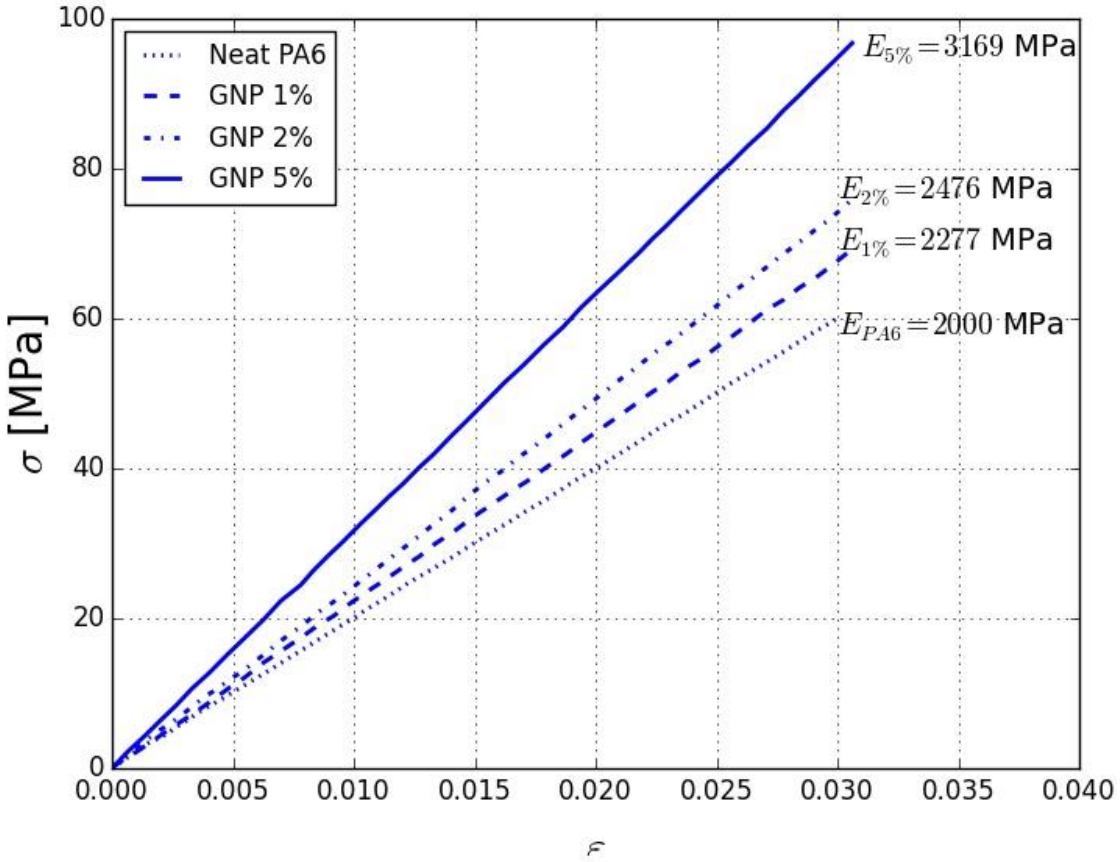

FIGURE 4. Effective stiffness versus the GNPs volume fraction

Next, a sensitivity analysis is performed with the AR variation. For a selected GNPs volume fraction, such as vf=1%, Table 4 summarizes the results of the AR variation. The effective Young modulus increases until value of AR=0.00125. Beyond that value of AR, a decrease has been noticed for the Young modulus. This decrease is explained by the non-uniform distribution of the graphene within the RVE as shown in Figure 3.

TABLE4: Effective Young modulus of a Polyamide PA6/GNPs composite versus the AR

Aspect Ratio [AR]	Effective Young modulus E [MPa]
0.054	2277
0.015	2357
0.008	2322
0.004	2286
0.002	2504
0.00125	2678
0.001	2163
0.00042	2136
0.00022	2140
0.00015	2122

For more realistic situations, a nanocomposite based on the AR distribution from Table5 is considered. A weighted average of the stiffness in Table 4 gives: E = 2213 MPa. This value is about 11 % of increase of the stiffness, with respect to the neat PA6 and this value is near to that obtained with AR=0.001. This stiffness value is considered as reference for the evaluation of the debonding of the nanocomposite. Using the maximum values of the debonding stresses between polyamide PA6 and GNPs in Table 1, the debonding response of the nanocomposite was determined for different volume fraction of GNPs. In addition, the maximum value of the supported load is obtained for the nanocomposite. Figure 5 depicts the contour plot of the observed debonding phenomena between the GNPs and the polyamide PA6.

TABLE 5: AR distribution for GNPs

%vol	5	5	20	20	20	10	10	5	5
AR	0.002	0.00125	0.001	0.00042	0.00033	0.000222	0.0001695	0.0001428	0.00125

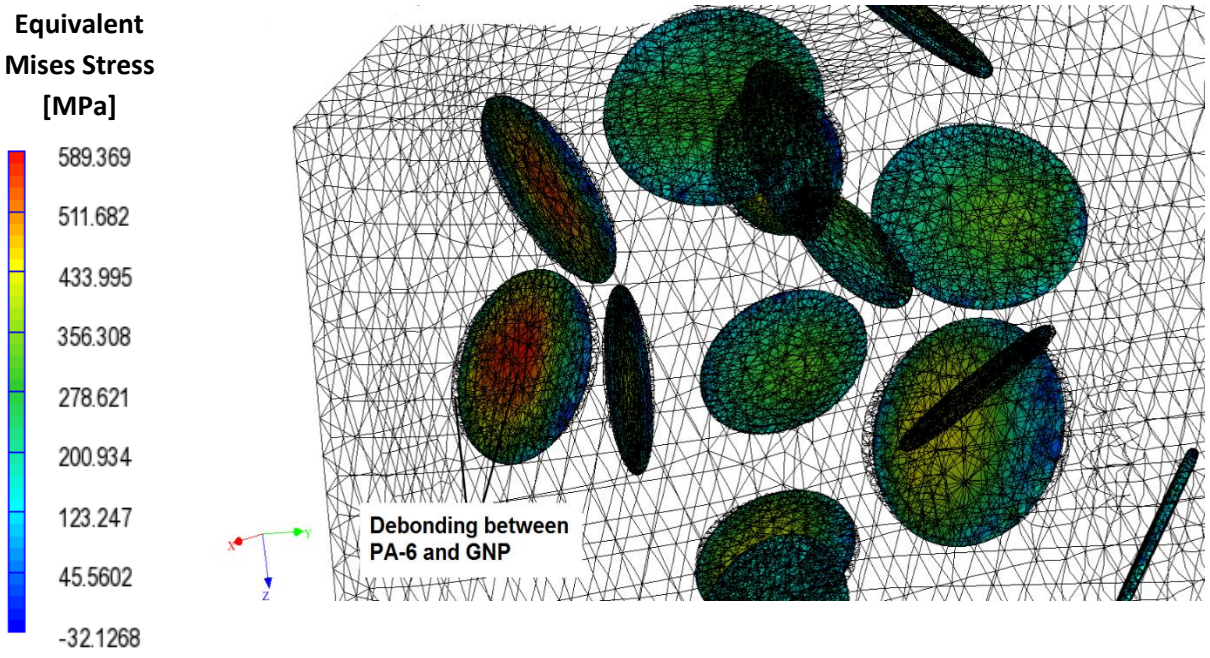

FIGURE 5. Contour plot of debonding phenomena at the interface between the polyamide PA6 and GNPs.

Results of such analysis are shown in Figure 6. One can notice the decrease of the Young modulus from the perfectly bonded composite to the debonding composite. A drop from $E_{Perfect}$ = 2200 MPa to $E_{Debonding}$=2080 MPa is noticed due to the imperfection assumed at the interface. This debonding curve will be used in the final phase for the virtual characterization of the composite with short glass fibers.

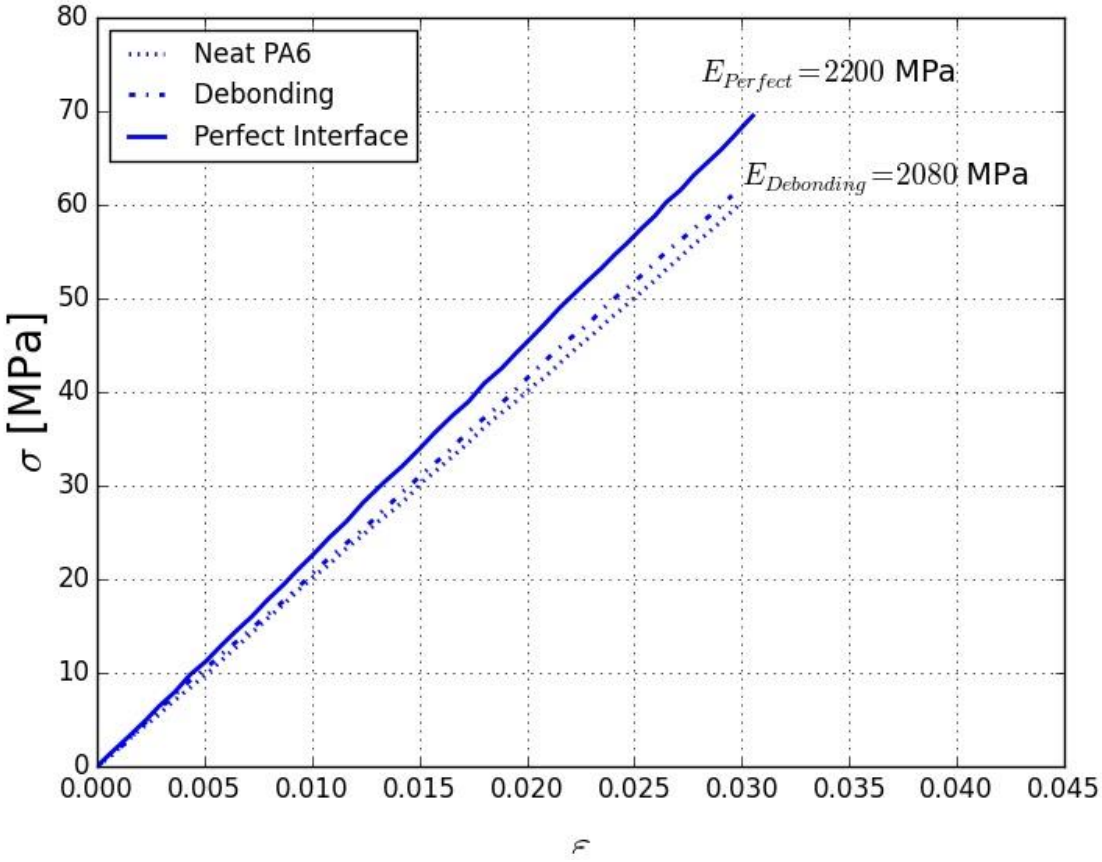

FIGURE 6: Stress-strain response for perfectly-bonded and debonding the GNPs/POLYAMIDE PA6 nanocomposite

GNPs/Epoxy nanocomposites

A volume fraction Vf=2% of GNPs is dispersed within an epoxy matrix. The interface GNP/Epoxy is considered perfectly bonded. For a sake of a sensitivity analysis, different ARs have been studied. Results of the homogenized properties are presented in Table 6.

TABLE 6. Effective Young modulus of a GNPs/Epoxy versus the AR

Aspect Ratio [AR]	Effective Young modulus E [MPa]
0.002	3587
0.00125	3529
0.001	3862
0.00042	3700

0.00022	3430
0.00015	3450

Based on the same procedure used above for the GNPs/Polyamide PA6, a weighted average stiffness from AR= [0.002, 0.00015] is obtained such as: E = 3651 MPa. This value corresponds nearly to 8 % of increase of the stiffness for the epoxy without GNPs. These values are used as reference for the evaluation of the debonding of the nanocomposite based on the AR distribution given in Table 5. Table 7 summarizes the obtained results in terms of the maximum stress at the debonding versus the neat epoxy matrix.

TABLE 7: Maximum stress at the debonding "Smax" for GNPs/Epoxy

	Debonding with 2% GNPs	Epoxy	Error Δ%
Smax[(a)] [MPa]	93	85	9

[(a)]Smax : Maximum stress at the debonding.

Three-phases GNPs based fibers reinforced polymer nanocomposites

The 3-phases nanocomposites, consisting on GNPs/Polyamide PA6/SGFs and GNP/Epoxy/UCFs, are considered for a virtual characterization. The material properties and volume fractions of constituents for both nanocomposites are given in Table 2. The methodology used to determine the characteristics of the 3-phases nanocomposite is shown in Figure 7.

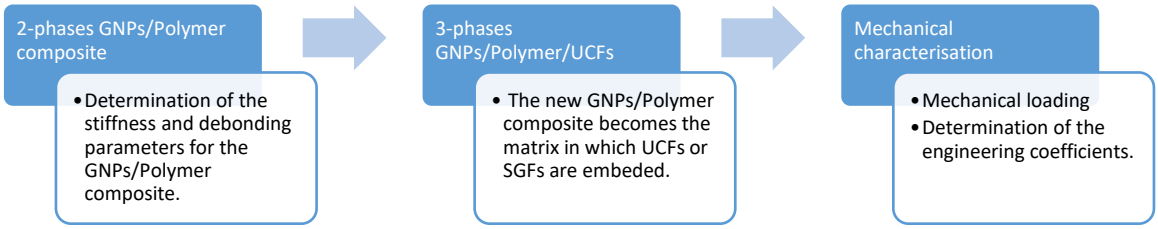

FIGURE 7: Methodology for a virtual characterization of the 3-phases nanocomposite

The calculations were also performed on the neat polyamide PA6 and epoxy, both without GNPs. The final results are shown in the following Table 8 and Table 9 respectively for GNPs/Polyamide PA6/SGFs and GNPs/Epoxy/UCFs:

TABLE 8: Effective properties for the SGFs/Polyamide PA6 and GNPs/Polyamide PA6/SGFs nanocomposites

	SGFs/Polyamide PA6	GNPs/Polyamide PA6/SGFs	Error Δ%
Effective Young modulus E [MPa]	13370	14000	4.7
Effective shear modulus G [MPa]	5129	5416	5.6
Effective Poisson's ratio ν	0.30	0.30	-
Density ρ[g/cm^3]	1.94	1.95	
Shear strength S [MPa]	184	179	-2.7
Deformation ε%	1.4%	1.4%	-

TABLE 9: Effective properties for the UCFs/Epoxy and GNPs/Epoxy/UCFs nanocomposites

	UCFs/Epoxy	GNPs/Epoxy/UCFs	Error Δ%
Effective Young modulus E^L [MPa]	130000	130500	0.4
Effective Young modulus E^T [MPa]	10890	12000	10
Effective shear modulus G^{LT} [MPa]	3743	4160	11
Effective Poisson's ratio ν^{LT}	0.45	0.45	
Density ρ[g/cm^3]	1.5	1.52	
Tensile strength X^L [MPa]	2000	2005	0.25
Tensile strength Y^T [MPa]	100	116	16
Shear strength S^{LT} [MPa]	124	129	4
Deformation ε% (X^L)	1.5%	1.5%	-

^{L} Longitudinal direction, ^{T} Transversal direction, ^{LT} in-plane direction.

From both tables, an increase is seen with the addition of the GNPs on the effective engineering coefficients. Indeed, for the GNPs/Polyamide PA6/SGFs, the GNPs have increased the Young and shear moduli up to 4.7% and 5.6% respectively. While a significant enhancement is observed for the GNPs/Epoxy/UCFs nanocomposite in the transversal direction (up to 10% for the transverse Young modulus and up to 11% for the shear modulus), a weak variation has been achieved in the longitudinal direction with only up to 0.4% increase of the longitudinal Young modulus. Indeed, the mechanical behavior of the composite is fiber-dominant in the longitudinal direction. That explains the weak enhancement achieved by the addition of GNPs within the epoxy matrix. In the transversal direction, the mechanical behavior of the composite is matrix-dominant. That explains the increase of the mechanical properties due to the reinforcement of the epoxy by the GNPs.

In terms of failure parameters i.e the tensile strength in longitudinal direction X^L, in the transversal direction Y^T, and in the shear strength S^{LT}, a similar trend compared to engineering coefficients has been obtained. GNPs have led to significant enhancement of these parameters in the transversal direction of the fibers while no significant increase has been noticed in the longitudinal direction.

Failure analysis of a CF laminate under a Mode I loading

A laminate cross ply [0/90/0] is considered as shown by Figure 8. The thickness for each ply is given by t=0.15 mm. For this laminate and using the Digimat 2016.0 [33], the in-situ transverse tensile strength has been determined for the first ply at 0° and second ply at 90°.

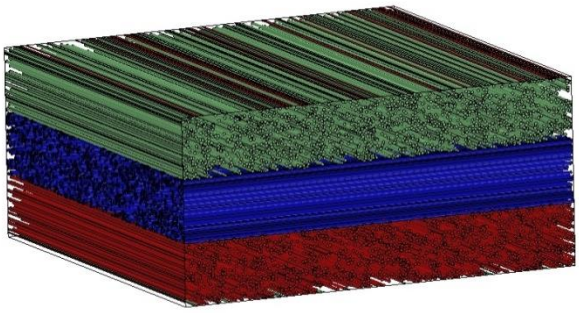

Figure 8: UCFs Cross ply laminate

For UCFs reinforced with and without GNP, the following values for the in-situ transverse tensile strength are presented in Table 10.

TABLE 10: In-Situ transverse tensile strength for cross ply laminate

	With GNP	Without GNP
$Y^{is}_{t\,[0]}$ [MPa]	479	470
$Y^{is}_{t\,[90]}$ [MPa]	783	780

Based on analytical formulations [44], an expression of the in-situ transverse tensile strength for unidirectional UD laminate yields:

$$Y_t^{is} = \sqrt{\frac{8G_{IC}(L)}{\pi t \Delta_{22}^0}} \tag{9}$$

where $G_{IC}(L)$ is the intralaminar longitudinal fracture toughness and L is the longitudinal dimension of the ply. t is the thickness of the ply and Δ_{22}^0 denotes a component of the crack tensor defined such as:

$$\Delta_{22}^0 = 2\left(\frac{1}{E_{22}} - \frac{\nu_{12}^2}{E_{11}}\right) \tag{10}$$

Using Equation (9) for the in-situ transverse tensile strength, it is possible to obtain, the interlaminar fracture toughness $G_{IC}(L)$ for the UD composite with and without GNPs.

Experimental determination of the intralaminar fracture toughness

The interlaminar fracture toughness G_{IC} is determined through the experimental test ASTM D5528 [45]. This test is related to the "Standard Test Method for Mode I Interlaminar Fracture Toughness of Unidirectional Fiber-Reinforced Polymer Matrix Composites". The experimental procedure shown by Figure 9, is concerned with GNPs/Epoxy/UCFs as well as UCFs/Epoxy. Three double cantilever beam DCB samples have been tested for each nanocomposite. Both mechanical extensometer and video extensometer (with a software post processing) are used for the strain measurement. Indeed, a dynamometer in automatic way determines the Load/Displacement curve and thanks to a software processing, the stiffness and fracture toughness are obtained. Tables 11- 12 summarize the experimental G_{IC} for both UCFs/Epoxy and GNPs/Epoxy/UCFs respectively. A comparison between the simulated and experimental responses is given by Table 13. The intralaminar fracture toughness G_{IC} has decreased up to 8.5 % for simulation and up to 2.4% for experiments. This can be explained by well-known uniform dispersion issues of GNPs.

TABLE 11: Experimental fracture toughness for UCFs/Epoxy

Characteristics	Sample 1	Sample 2	Sample 3
Strength [N]	52	48	47
Displacement [mm]	5.90	6.10	5.60
G_{IC} [mm.MPa]	5.75	5.49	4.94
Mean G_{IC} [mm.MPa]	5.39		
Standard Deviation	0.42		

TABLE 12: Experimental fracture toughness for GNPs/Epoxy/UCFs

Characteristics	Sample 1	Sample 2	Sample 3
Strength [N]	44	51	49
Displacement [mm]	5.50	6.10	5.90
G_{IC} [mm.MPa]	4.54	5.83	5.42
Mean G_{IC} [mm.MPa]	5.26		
Standard Deviation	0.66		

TABLE 13: Simulation versus Experimental fracture toughness

	Mode I fracture toughness G_{IC} [mm.MPa]		
	Simulation	Experiment	Standard deviation of experiments
GNPs/Epoxy/UCFs	6.02	5.26	0.66
UCFs/Epoxy	6.58	5.39	0.42

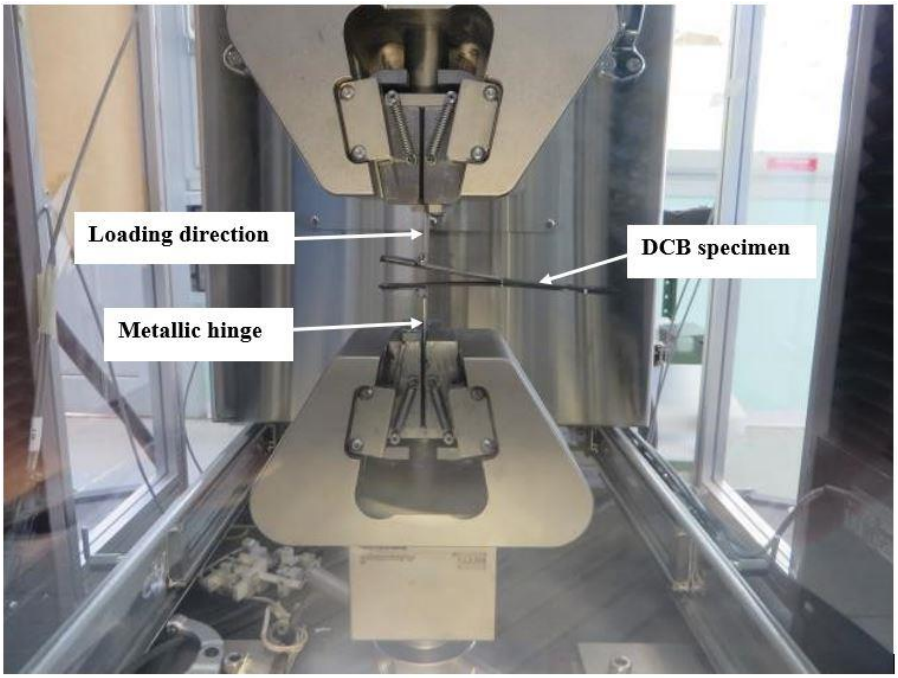

Figure 9: ASTM D5528 test for Mode I Interlaminar Fracture Toughness [45]

Interlaminar failure of a unidirectional laminate for automotive components

The 3-phases nanocomposites GNPs/Polyamide PA6/SGFs and GNPs/Epoxy/UCFs are both used in automotive structural parts such as the bumper beams or the anti-intrusion bars whose outer faces are manufactured in UCFs reinforced polymer laminates while SGFs reinforced polymer composites are used for the inner faces.

In this work, a numerical model of a bumper beam is considered for sake of a simulacrum as presented by Figure 10. The fundamental performance of the bumper beam is the energy absorption during a frontal impact crashworthiness. The outer part of this beam, realized with UCFs reinforced polymer, is a quasi-isotropic laminate with the stacking sequence [0/45/-45/-45/45/0]. The principal damage phenomena that contribute in crashworthiness events are the progressive failure of the plies (Intralaminar failure) and debonding of the plies (Interlaminar failure) [46]. Therefore, the distribution of the interlaminar stress in the laminate is of interest since it represents the fundamental aspect of the delamination phenomenon. For such a purpose, the ASTM D2344 [47] (Standard Test Method for Short-Beam Strength of Polymer Matrix Composite Materials and Their Laminates D2344 / D2344M – 16) test is performed for laminate both with and without GNPs. Results in Figure 11a present the distribution of the interlaminar stress in the transverse direction σ_{33} versus the displacement z. From the bottom surface z = 0 mm to nearly the middle z= 0.9 mm of the laminate, a decrease of σ_{33} is observed while it begins to increase from z=0.9 mm to the top z=1.8 mm. A similar trend has been obtained for the shear stress τ_{13} in Figure 11b with a decrease from the bottom surface to beyond z= 0.6 mm, following by an increase of the shear stress until

the top face z=1.8 mm. However, no-significant impact of the GNPs is noticed on the interlaminar stress distribution. This is explained by the slightly difference between performance obtained in Table 9. Indeed, the well-known problem of a uniform dispersion of the GNPs explains the decrease of the fracture toughness performance due to the clustering of GNPs within the epoxy matrix. The clustering represents a damage initiation point and therefore a parameter for the decrease of the fracture toughness

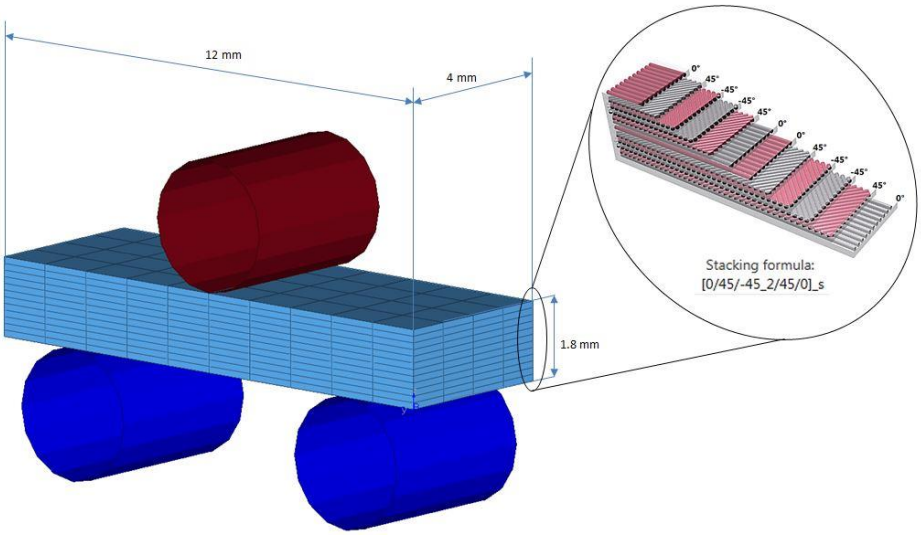

FIGURE 10: Simulation of the ASTM D2344[47] for a bumper beam

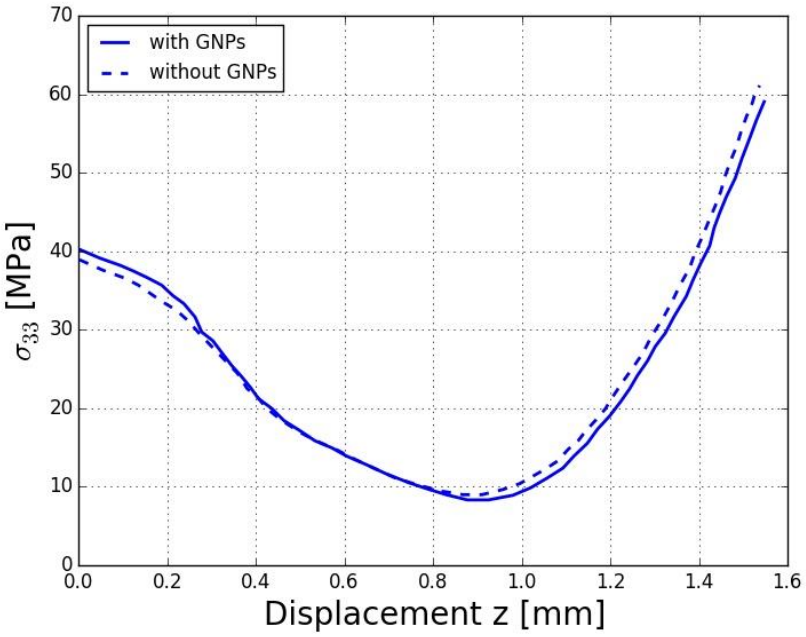

(a) Transverse intralaminar stress σ_{33} versus displacement

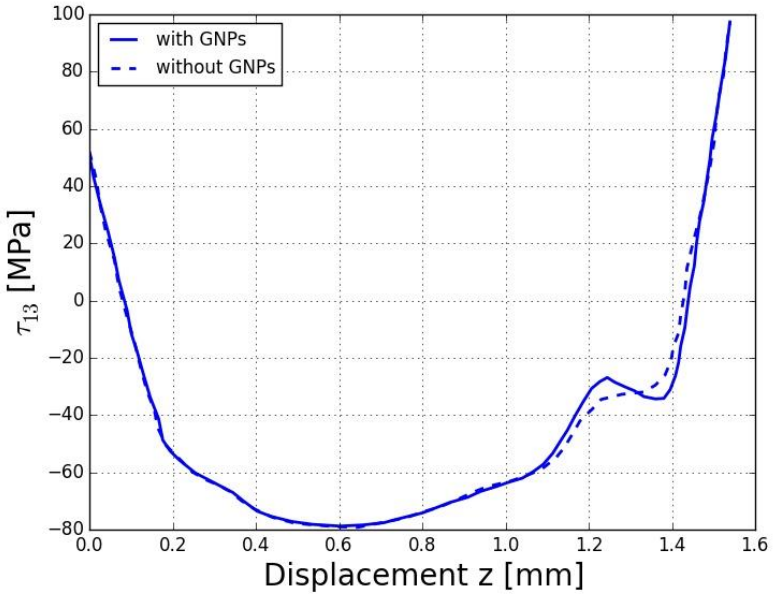

(b) Intralaminar shear stress τ_{13} versus displacement

FIGURE 11: Simulation results on the Interlaminar stress distribution

CONCLUSION

A multiscale simulation accounting for a cohesive debonding is developed for GNPs, reinforced by both SFGs and UCFs polymer laminate composites. The design parameters for such composites are the AR of the volume fraction of the GNPs. In addition, experiments based on the ASTM D5528 are performed with a confrontation of the intralaminar fracture toughness G_{IC} with the simulation results.

Results highlight the contribution of the GNPs which increases the effective mechanical response in terms of transversal Young modulus, transverse tensile strength useful in crashworthiness performance. Indeed, the addition of the GNPs increases up to 10% the transverse Young modulus and up to 11% the shear modulus as well as up to 16% the transverse tensile strength. This variation however remains very weak for longitudinal mechanical properties due to low resistance of the interface and the clustering phenomena as well as the difficulty of a uniform dispersion of the GNPs in the polymeric matrix. The intralaminar fracture toughness G_{IC} has decreased up to 8.5 % for simulation and up to 2.4% for experiments while no significant variation of the intralaminar stress distribution is obtained compared to a nanocomposite without GNPs. It is therefore necessary to realize the dispersion of quantities of the GNPs over the currently achievable 2% vol. whilst simultaneously ensuring the absence of clustering as well as a strong interface between GNPs and the matrix.

This work represents a first attempt for lightweighting the main structure of the vehicles by GNPs. For the R&D unit of FIAT Chrysler Automobile (FCA), it enables a development of a new methodology for virtual characterization of the UD ply. As a perspective, the quality of the interface between the GNPs and the

matrix will be addressed in further works with a focus on the electrical and thermal properties for automotive applications.

ACKNOWLEDGMENTS

The research leading to these results has received funding from the European Union Seventh Framework Program under grant agreement no. 604391 and from Horizon 2020 program under grant agreement no. 696656 Graphene Flagship.

REFERENCES

[1] Martorana B, Elmarakbi A, Veca A, Fondacaro D, Lambertini VG. Graphene-based materials: opportunities for multifunctional lightweight structures in automotive sector. *In: NANOTECHITALY*; **2015**.

[2] Inagaki M, Kim YA, Endo M. Graphene: preparation and structural perfection. *J Mater Chem*. **2011**; 21:3280–3294.

[3] Park S, Ruoff RS. Chemical methods for the production of graphenes. *Nat Nano*. **2009** Apr; 4(4):217–224.

[4] Soldano C, Mahmood A, Dujardin E. Production, properties and potential of graphene. *Carbon*. **2010**; 48(8):2127 – 2150.

[5] Ege D, Kamali AR, Boccaccini AR. Graphene Oxide Polymer Based Biomaterials. *Advanced Engineering Materials*. **2017**; 19(12):1700627.

[6] Huang WM, Sun WF, Chen GH, Tan L. Nanocavities Double the Toughness of Graphene–Polycarbonate Composite. *Advanced Engineering Materials*. **2014**; 17(3):299–304.

[7] King JA, Klimek DR, Miskioglu I, Odegard GM. Mechanical properties of graphene nanoplatelet/epoxy composites. *Journal of Applied Polymer Science*. **2013**; 128(6):4217–4223.

[8] Larsen RM, Jensen EA. Epoxy–graphite oxide nanocomposites: Mechanical properties. *Journal of Applied Polymer Science*. **2016**; 133(26).

[9] Lu X, Munief WM, Heib F, Schmitt M, Britz A, Grandthyl S, et al. Front End of Line Integration of Graphene Oxide for Graphene Based Electrical Platforms. *Advanced Materials Technologies*. **2018**; 3(4):1700318.

[10] Pokharel P, Bae H, Lim JG, Lee KY, Choi S. Effects of titanate treatment on morphology and mechanical properties of graphene nanoplatelets/high density polyethylene nanocomposites. *Journal of Applied Polymer Science*. **2015**; 132(23).

[11] Rafiee MA, Rafiee J, Srivastava I, Wang Z, Song H, Yu ZZ, et al. Fracture and Fatigue in Graphene Nanocomposites. *Small*. **2010**; 6(2):179–183.

[12] Veca LM, Meziani MJ, Wang W, Wang X, Lu F, Zhang P, et al. Carbon Nanosheets for Polymeric Nanocomposites with High Thermal Conductivity. *Advanced Materials*. **2009**; 21(20):2088–2092.

[13] Xu Z, Gao C. In situ Polymerization Approach to Graphene-Reinforced Nylon-6 Composites. *Macromolecules*. **2010**; 43(16):6716–6723.

[14] Zhang WL, Park BJ, Choi HJ. Colloidal graphene oxide/polyaniline nanocomposite and its electrorheology. *Chem Commun*. **2010**; 46:5596–5598.

[15] Rao CVSK. A note on fracture toughness of multiphase materials. *Engineering Fracture Mechanics*. **1983**; 18(1):35 – 38.
[16] Yaghoobi A, Chorzepa MG, Kim SS, A S. Mesoscale Fracture Analysis of Multiphase Cementitious Composites Using Peridynamics. *Materials* (Basel, Switzerland). **2017**; 10(2):162.
[17] Turteltaub S, van Hoorn N, Westbroek W, Hirsch C. Multiscale analysis of mixed-mode fracture and effective traction-separation relations for composite materials. *Journal of the Mechanics and Physics of Solids*. **2018**; 117:88 – 109.
[18] Saghafi H, Brugo T, Minak G, Zucchelli A. The effect of PVDF nanofibers on mode-I fracture toughness of composite materials. *Composites Part B: Engineering*. **2015**; 72:213 – 216.
[19] Fu SY, Feng XQ, Lauke B, Mai YW. Effects of particle size, particle/matrix interface adhesion and particle loading on mechanical properties of particulate-polymer composites. *Composites Part B: Engineering*. **2008**; 39(6):933 – 961.
[20] Ji XL, Jing JK, Jiang W, Jiang BZ. Tensile modulus of polymer nanocomposites. *Polymer Engineering & Science*. **2002**; 42(5):983–993.
[21] Reynaud E, Jouen T, Gauthier C, Vigier G, Varlet J. Nanofillers in polymeric matrix: a study on silica reinforced PA6. *Polymer*. **2001**; 42(21):8759 – 8768.
[22] Wetzel B, Haupert F, Zhang MQ. Epoxy nanocomposites with high mechanical and tribological performance. *Composites Science and Technology*. **2003**; 63(14):2055 – 2067.
[23] Ou Y, Yang F, Yu ZZ. A new conception on the toughness of nylon 6/silica nanocomposite prepared via in situ polymerization. *Journal of Polymer Science Part B: Polymer Physics*. **1998**; 36(5):789–795.
[24] Fedele R, Milani G. Assessment of bonding stresses between FRP sheets and masonry pillars during delamination tests. *Composites Part B: Engineering*. **2012**; 43(4):1999 – 2011.
[25] Šejnoha M, Zeman J. Overall viscoelastic response of random fibrous composites with statistically quasi uniform distribution of reinforcements. *Computer Methods in Applied Mechanics and Engineering*. **2002**; 191(44):5027 – 5044.
[26] Cecchi A, Milani G, Tralli A. Validation of Analytical Multiparameter Homogenization Models for Out-of-Plane Loaded Masonry Walls by Means of the Finite Element Method. *Journal of Engineering Mechanics*. **2005**; 131(2):185–198.
[27] Cecchi A, Milani G, Tralli A. In-plane loaded CFRP reinforced masonry walls: mechanical characteristics by homogenisation procedures. *Composites Science and Technology*. **2004**; 64(13):2097 – 2112.
[28] Azoti W, Elmarakbi A. Constitutive modelling of ductile damage matrix reinforced by platelets-like particles with imperfect interfaces: Application to graphene polymer nanocomposite materials. *Composites Part B: Engineering*. **2017**; 113:55 – 64.
[29] Azoti WL, Elmarakbi A. Multiscale modelling of graphene platelets-based nanocomposite materials. *Composite Structures*. **2017**; 168:313 – 321.
[30] Elmarakbi A, Azoti W. In: Mechanical Prediction of Graphene-Based Polymer Nanocomposites for Energy-Efficient and Safe Vehicles. *Micro and Nano Technologies. Elsevier*; **2018**. p. 159 – 177.
[31] Elmarakbi A, Azoti W. In: State of the Art on Graphene Lightweighting Nanocomposites for Automotive Applications. *Micro and Nano Technologies. Elsevier*; **2018**. p. 1 – 23.
[32] Elmarakbi A, Azoti W, Serry M. Multiscale modelling of hybrid glass fibres reinforced graphene

platelets polyamide {PA6} matrix composites for crashworthiness applications. *Applied Materials Today*. **2017**; 6:1 – 8.

[33] Company MS. Digimat User's Manual, E-xstream Engineering; **2016**.

[34] Vieville P, Bonnet AS, Lipinski P. Modelling effective properties of composite materials using the inclusion concept. General considerations. *Arch Mech*. **2006**; 58(3):207–239.

[35] Safaei M, Sheidaei A, Baniassadi M, Ahzi S, Mashhadi MM, Pourboghrat F. An interfacial debonding-induced damage model for graphite nanoplatelet polymer composites. *Computational Materials Science*. **2015**; 96, Part A:191 – 199.

[36] Huang J, Uhrig M, Weber U, Schmauder S. Numerical Simulation of Mechanical Properties of Nano Particle Modified Polyamide 6 via RVE Modeling. *Journal of Materials Science and Chemical Engineering*. **2015**; 3:95–102.

[37] DSM. Akulon F-X9215-PA6 DSM Engineering Plastics; **2018**.

[38] Hartman D, Greenwood ME, Miller DM. High Strength Glass Fibers. Agy; **2006**.

[39] Toray Carbon Fibers America I. Technical T300 DATA SHEET; **2018**.

[40] Mark JE. Polymer data handbook. Oxford University Press; **1999**.

[41] Lee C, Wei X, Kysar JW, Hone J. Measurement of the Elastic Properties and Intrinsic Strength of Monolayer Graphene. *Science*. **2008**; 321(5887):385–388.

[42] Cho J, Luo JJ, Daniel IM. Mechanical characterization of graphite/epoxy nanocomposites by multi-scale analysis. *Composites Science and Technology*. **2007**; 67(1112):2399 – 2407.

[43] Xiao JR, Gama BA, Jr JWG. An analytical molecular structural mechanics model for the mechanical properties of carbon nanotubes. *International Journal of Solids and Structures*. **2005**; 42:3075 – 3092.

[44] Pinho ST, Davila CG, Camanho PP, Iannucci L, Robinson P. Failure Models and Criteria for FRP Under In-Plane or Three-Dimensional Stress States Including Shear Non-Linearity. NASA Langley Research Center; Hampton, VA, United States; **2005**.

[45] D5528-13 A. Standard Test Method for Mode I Interlaminar Fracture Toughness of Unidirectional Fiber-Reinforced Polymer Matrix Composites D5528 - 13; **2013**.

[46] Shyr TW, Pan YH. Impact resistance and damage characteristics of composite laminates. *Composite Structures*. **2003**; 62(2):193 – 203.

[47] D2344M-16 AD. Standard Test Method for Short-Beam Strength of Polymer Matrix Composite Materials and Their Laminates D2344 / D2344M - 16; **2016**.

GRAPHICAL ABSTRACT

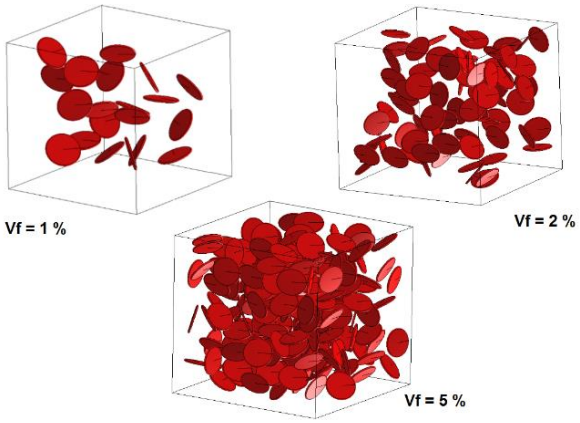

2-phases nanocomposites

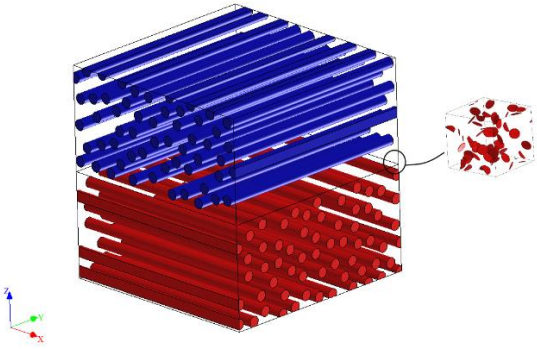

3-phases nanocomposites

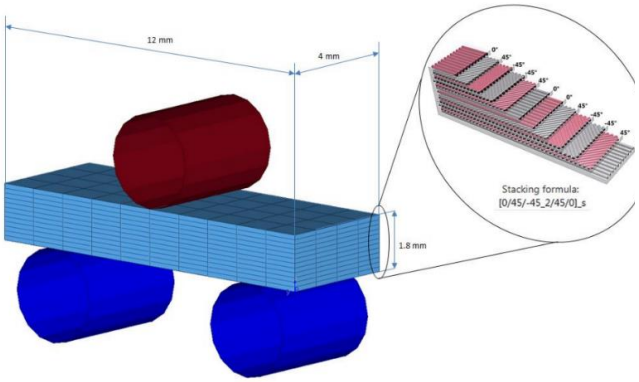

Multiscale simulation

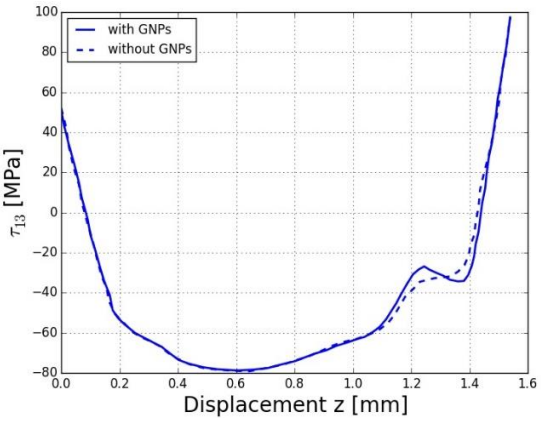

Intralaminar stress distribution